Diagn Interv Radiol 2026; DOI: 10.4274/dir.2026.263832

BREAST IMAGING

ORIGINAL ARTICLE

Contrast-enhanced mammography and breast magnetic resonance imaging in invasive lobular carcinoma: a comparative analysis of morphological features and enhancement kinetics

Güliz Yılmaz
Şebnem Örgüç

Manisa Celal Bayar University Faculty of Medicine, Department of Radiology, Manisa, Türkiye

PURPOSE

This study aimed to compare the diagnostic performance of contrast-enhanced mammography (CEM) and dynamic contrast-enhanced breast magnetic resonance imaging (MRI) in the preoperative evaluation of invasive lobular carcinoma (ILC) in terms of lesion size measurement, morphological characteristics, and enhancement kinetics.

METHODS

In this retrospective single-center study, 62 lesions from 46 patients with histopathologically confirmed ILC who underwent both CEM and MRI between February 2021 and December 2024 were analyzed. Lesion size was measured based on the maximum diameter of the index lesion on both modalities. Morphological patterns, including architectural distortion, mass and non-mass enhancement (NME) patterns, and lesion conspicuity, were analyzed according to the American College of Radiology Breast Imaging Reporting and Data System v2025 lexicon. Enhancement kinetics on CEM were categorized as persistent, plateau, or washout based on visual assessment of early- and delayed-phase images and compared with MRI kinetic curve types.

RESULTS

The mean age of the patients was 50.6 ± 10.1 years, and multifocal or bilateral disease was observed in 35% of cases. Lesions presented as a mass in 71%, NME in 50%, and a small mass in 37.1% of cases. Both CEM and MRI demonstrated comparable accuracy in measuring the size of the index lesion (intraclass correlation coefficient range: 0.995–0.997; $P < 0.001$). A high level of agreement was found between CEM and MRI in kinetic curve patterns (Kappa: 0.764; $P < 0.001$). The sensitivity of CEM was 94.1% for type 1, 89.2% for type 2, and 62.5% for type 3 enhancement patterns. Architectural distortion was significantly more frequent in type 2 and type 3 patterns. High conspicuity was the most common finding on CEM, whereas low conspicuity was predominantly observed in type 1 lesions. MRI was superior for the evaluation of extra-mammary extension, soft tissue involvement, and axillary lymph nodes.

CONCLUSION

CEM demonstrates diagnostic performance comparable with MRI in assessing lesion size, morphology, and enhancement kinetics in ILC. It represents a valuable alternative imaging modality in cases where MRI is contraindicated or limited in availability. However, MRI remains the gold standard for investigating NME and extra-mammary disease extension.

CLINICAL SIGNIFICANCE

CEM provides diagnostic accuracy comparable with MRI in assessing lesion size, morphology, and additional lesions in ILC. Its high sensitivity, shorter examination time, and cost-effectiveness make it a valuable alternative imaging modality, particularly in cases where MRI is contraindicated or limited in availability. Furthermore, the integration of CEM into clinical practice may contribute to improved preoperative assessment.

KEYWORDS

Contrast-enhanced mammography, enhancement kinetics, invasive lobular carcinoma, lesion conspicuity, magnetic resonance imaging

Corresponding author: Güliz Yılmaz

E-mail: sglz.ylmz@gmail.com

Received 08 January 2026; revision requested 28 January 2026; last revision requested 13 April 2026; accepted 16 April 2026.

Epub: 29.04.2026

Publication date:

DOI: 10.4274/dir.2026.263832

You may cite this article as: Yılmaz G, Örgüç Ş. Contrast-enhanced mammography and breast magnetic resonance imaging in invasive lobular carcinoma: a comparative analysis of morphological features and enhancement kinetics. *Diagn Interv Radiol*. 29 April 2026 DOI: 10.4274/dir.2026.263832 [Epub Ahead of Print].

Invasive lobular carcinoma (ILC) represents the second most common subtype of breast cancer, following invasive ductal carcinoma (IDC). It is distinguished by a unique growth pattern characterized by single-file infiltration, minimal alteration of normal tissue architecture, and a minimal or absent desmoplastic stromal response, often resulting in subtle clinical and radiological findings. This biological behavior leads to frequent underestimation of disease extent with conventional imaging modalities, such as mammography (MG) and ultrasound (US), particularly in patients with dense breast parenchyma.[1,2] Due to its clinically silent presentation and the absence of a palpable mass in many cases, ILC is frequently diagnosed at a later stage, especially by the conventional imaging modalities, and with a larger tumor size than IDC.[3]

Due to its often multifocal, multicentric, and bilateral nature, accurate preoperative staging is crucial in ILC to reduce re-excision rates and optimize surgical management. Magnetic resonance imaging (MRI) has been widely recommended for ILC cases because of its high sensitivity for lesion detection in the ipsilateral and contralateral breast and its improved estimation of tumor extension, which cannot be observed by US or conventional MG. However, its limited specificity, higher cost, and reduced accessibility restrict its universal application.[1,2,4]

Main points

- Contrast-enhanced mammography (CEM) and breast magnetic resonance imaging (MRI) demonstrate comparable performance in assessing lesion size, morphology, enhancement kinetics, and additional lesions in patients with invasive lobular carcinoma (ILC).
- CEM shows a high level of agreement with MRI in the classification of enhancement kinetics (Kappa: 0.764), with particularly strong sensitivity for type 1 and type 2 enhancement curves.
- High conspicuity and architectural distortion on CEM are significantly associated with more aggressive enhancement kinetics (type 2 and type 3 curves), whereas type 1 lesions more frequently showed low conspicuity.
- CEM represents a valuable alternative modality to MRI, offering shorter examination time, lower cost, and high diagnostic accuracy in the preoperative evaluation of ILC, particularly when MRI is contraindicated or unavailable.

Contrast-enhanced MG (CEM) represents a new era in functional imaging that combines conventional MG with intravenous contrast administration to highlight vascularized tissue. Recent evidence suggests that CEM may offer diagnostic performance comparable with MRI, with favorable specificity and practicality, particularly in resource-limited or MRI-contraindicated settings.[4,5] In addition to screening-detected lesions, the study population also included symptomatic patients presenting with palpable breast masses. Nevertheless, the literature remains limited regarding direct modality comparisons in the specific setting of ILC, especially in terms of lesion multiplicity, bilaterality, and size concordance with pathology.[2,5] CEM would be an alternative imaging modality to MRI to show non-mass enhancement (NME), small mass (SM), and additional mass in the ipsilateral or contralateral breast in ILC cases due to its distinctive biological and imaging characteristics.

In this study, we retrospectively compare CEM and dynamic contrast-enhanced MRI findings in patients with histopathologically confirmed ILC.

Methods

Ethical approval for this retrospective study was obtained from the Institutional Review Board of Celal Bayar University Faculty of Medicine, Health Sciences Ethics Committee (decision number: 20.478.486/3585, date: 26.11.2025).

This retrospective, single-center study was performed at the Radiology Department of Manisa Celal Bayar University Hafsa Sultan Hospital between February 2021 and December 2024. The study included patients histopathologically diagnosed with ILC who underwent both CEM and breast MRI.

A total of 65 patients who had been histopathologically diagnosed with ILC and had undergone CEM were reviewed through the archive system. These patients included those referred to the clinic with palpable breast masses as well as those in whom NME or SM were detected during breast screening. CEM was performed on all patients who were referred with suspicion of a breast mass, whereas it was performed in addition to routine bilateral MG and US when US findings were suspicious in cases who were undergoing screening.

Among the 65 patients who underwent CEM, 46 were included in the study, and 19 patients were excluded due to contraindications for MRI, such as obesity, claustrophobia, or other medical limitations. All included patients provided written informed consent. In this study, a total of 62 lesions from 46 patients with a confirmed diagnosis of ILC were retrospectively evaluated using both CEM and breast MRI (Figure 1).

CEM was performed using a dual-energy digital MG system (Pristina, GE Healthcare Buc, France). A nonionic, low-osmolar iodinated contrast agent was administered intravenously at a dose of 1.5 mL/kg (maximum 100 mL) using an automatic injector at a rate of 3 mL/s, followed by a 20 mL saline flush. Image acquisition began 1.5–2 minutes after the start of injection, starting with the breast affected by the pathology. Craniocaudal and mediolateral oblique (MLO) views of both breasts were obtained using both low- and high-energy exposures. Rather than a routine protocol for all patients, in suspicious cases, as in the current study, a second MLO view of the affected breast was acquired as a late-phase image at the end of the examination. Image acquisition was completed in approximately 5 minutes, depending on patient compliance.

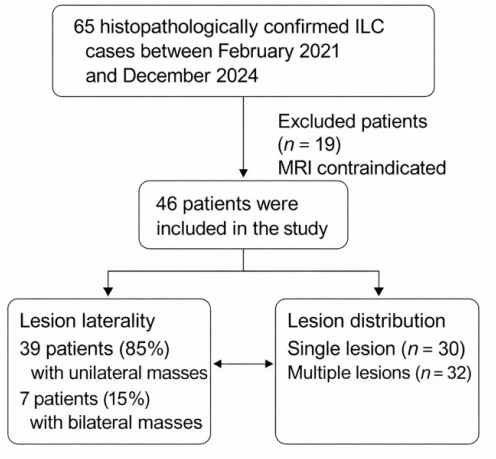

Figure 1. Flowchart of patient selection. ILC, invasive lobular carcinoma; MRI, magnetic resonance imaging.

This late-phase acquisition allowed for the assessment of enhancement kinetics (persistent, plateau, or washout), facilitating a more comprehensive comparison with dynamic contrast-enhanced MRI findings.

CEM was not performed in patients with a history of allergy to contrast agents (iodinated or gadolinium-based), renal failure, or pregnancy. Low-energy images were acquired at 28–32 kVp, and high-energy images at 45–49 kVp, with the filtration material and exact kVp settings automatically selected by the device. Recombined images were generated automatically by the system, highlighting and enhancing areas while suppressing background breast parenchyma. Neoangiogenesis of the tumor could be evaluated by these CEM images, as in MRI.

Breast MRI was performed using a 1.5 Tesla MRI machine (Signa HDx; General Electric, Madison, WI, USA) system with an 8-channel breast coil in the prone position. Breast MRI was performed after a lesion was detected on CEM, regardless of menstrual cycle phase, with an interval of up to 10 days (range: 7–10 days) between the two examinations. Standard sequences included precontrast axial T1-weighted fast spin echo, sagittal fat-saturated T2-weighted, diffusion-weighted imaging, and postcontrast sagittal fat-suppressed three-dimensional T1-weighted images (the VIBRANT sequence). After acquisition, all data were transferred to a workstation (Advantage Windows 4.4, GE Healthcare), where the kinetic curve types were created using the software. All images were evaluated by the same radiology specialist (14 years of experience, G.Y.) under the supervision of a senior radiology specialist (30 years of breast imaging experience, Ş.Ö.)

Performing both CEM and MRI in all patients is not part of the routine clinical protocol at the study institution. However, during the initial phase of CEM implementation, MRI was more frequently performed as a complementary imaging modality while institutional experience with CEM was being established. This approach enabled a direct comparison between the two modalities in patients diagnosed with ILC.

The diagnostic sequence typically began with CEM upon clinical suspicion of a breast lesion, followed by an immediate core needle biopsy for histopathological confirmation. In cases where ILC was diagnosed, breast MRI was subsequently performed to assess disease extent further. During the initial phase of the study, MRI was more routinely conducted to validate CEM findings as institutional experience was accumulating. The mean interval between initial imaging and biopsy was 2–3 days.

Morphological evaluation was performed in accordance with the American College of Radiology Breast Imaging Reporting and Data System (ACR BI-RADS®) lexicon and focused on features characteristic of ILC, including architectural distortion, mass versus NME patterns, and lesion distribution. Additionally, microcalcifications were analyzed on low-energy CEM images and categorized according to the BI-RADS descriptors. For each case, the presence or absence of associated enhancement on recombined CEM images was documented, and these findings were correlated with breast MRI. Although MRI provided high-resolution enhancement data, its inability to verify the morphological details of microcalcifications was specifically evaluated as a comparative parameter between the two modalities.

Pathological findings in CEM and MRI were categorized as mass, NME, or SM. Among these findings, SM was defined as a small enhancing spot < 1 cm in diameter that does not exhibit mass-like features, and NME was evaluated either as an isolated finding without a mass or as an associated pattern surrounding an SM or a mass. In cases presenting multiple lesions, the largest non-index lesion was selected as the representative additional focus for practical purposes and to maintain statistical robustness. This approach focused the analysis on the most clinically significant SMs that primarily impact preoperative staging and surgical decision-making. Lesion size was measured along the longest axis in the view showing the greatest extent. For NME, measurement was performed on the recombined image in the view where enhancement appeared most extensive. In cases of a mass with accompanying NME, the lesion size was calculated as the sum of both components. Index lesions and any additional lesions in the ipsilateral or contralateral breast were compared with both modalities. The selection of only the largest non-index lesion as a representative additional focus was intended to maintain statistical independence and prevent the bias associated with analyzing multiple dependent data points from a single patient. Extramammary extension, including nipple–areolar complex involvement, subcutaneous tissue involvement, and pectoral muscle invasion, was assessed visually on both CEM and MRI based on contrast enhancement patterns and morphological continuity with adjacent structures. Axillary lymph node was evaluated using established morphological criteria, including cortical thickening, loss or displacement of the fatty hilum, rounded configuration, and asymmetric enlargement. A modality-based comparison was performed to evaluate detection and visualization differences between CEM and MRI.

Images were interpreted in accordance with the ACR BI-RADS® 2025 manual.[6] Low-energy images were evaluated using BI-RADS criteria. On recombined images, lesion conspicuity relative to background parenchymal enhancement (BPE) was rated as low, moderate, or high. Low conspicuity was defined as lesion enhancement equal to or only slightly above BPE, whereas high conspicuity referred to markedly stronger enhancement. Architectural distortion was analyzed on low-energy CEM images.

Enhancement kinetics were assessed differently for each modality. MRI kinetics were determined quantitatively using automated curve generation on a dedicated workstation (AW 4.4, GE Healthcare). Enhancement kinetics on CEM were assessed by comparing early and delayed phase recombined images and classified into three patterns—persistent (type 1), plateau (type 2), and washout (type 3)—based on relative changes in enhancement intensity. This visual categorization was performed by two experienced radiologists to mirror the MRI kinetic types, facilitating a standardized comparative framework while acknowledging the qualitative nature of current CEM kinetic assessments compared with MRI software-based analysis.

Statistical analysis

Data were analyzed using IBM SPSS Statistics Standard Concurrent User V30 (IBM Corp., Armonk, NY, USA). Descriptive statistics were expressed as counts (n), percentages (%), means ± standard deviation, and minimum–maximum values. Agreement between MRI and contrast-enhanced spectral MG (CESM) findings was evaluated using the kappa coefficient. Comparisons of categorical variables across CESM and MRI types were performed using the Fisher–Freeman–Halton exact test. Where statistically significant, subgroup analyses were conducted using Bonferroni-adjusted two-proportion Z-tests. A P value of < 0.05 was considered statistically significant. Since three pairwise comparisons were performed, the Bonferroni-adjusted significance level was set at 0.05/3: 0.017.

Results

The age range of the 46 patients included in the study was 33–74 years, with a mean age of 50.6 ± 10.1 years. A single lesion was observed in 30 (65%) of the 46 cases, and multiple lesions (n = 62) were determined in 16 patients (35%), located either in the same or contralateral breast. In cases with multiple lesions, the largest non-index lesion was also included in the study as an additional focus. As a result, a total of 62 lesions were analyzed, consisting of 32 multifocal/multicentric lesions and 30 single lesions. Lesions were bilateral in 7 patients (15%), and in 39 patients (85%), the lesions were detected in the ipsilateral breast. Axillary lymph nodes were detected in 17 of the 46 patients (37%) on both CEM and MRI. In 9 of these cases, lymph nodes were more clearly visualized on MRI. In 1 additional patient (2%), lymphadenopathy was detected only on MRI. No axillary lymph nodes were identified on either modality in 28 patients (61%). Extramammary findings, including nipple–areolar complex involvement, subcutaneous tissue involvement, and/or pectoral muscle invasion, were observed in 10 patients (21.7%), with MRI providing superior visualization compared with CEM.

Index lesions were identified on both CEM and MRI in all included cases, although MRI demonstrated superior visualization of extramammary extension and axillary lymph nodes. Architectural distortion and lesion conspicuity were primarily evaluated on CEM low-energy images, whereas enhancement kinetics were assessed on both modalities.

Lesion size measurements obtained from CEM and MRI demonstrated excellent inter-modality agreement (intraclass correlation coefficient range: 0.995–0.997; $P < 0.001$).

Morphological features of the lesions diagnosed as ILC were defined on both CEM and MRI and evaluated in terms of shape, size, and pattern. Among the lesions, 44 (71.0%) presented as masses, 31 (50.0%) as NME, and 23 (37.1%) as SM. These enhancement patterns were observed either as single findings or in various combinations, leading to overlapping percentages. Detailed analysis revealed that the index lesion most frequently presented as an isolated mass in 25 lesions (40.3%). On CEM, this was followed by patterns involving NME with associated SM (19.4%, n = 12), mass with accompanying NME (17.7%, n = 11), and combined mass, NME, and SM (8.1%, n = 5). Isolated NME, isolated SM, and mass with SM were each observed in 3 cases (4.8%) (Table 1).

Microcalcifications were identified in 10 patients (21.7%) using low-energy CEM. Among these, 4 cases exhibited subtle microcalcifications within the primary ILC mass. Additional findings included scattered calcifications associated with benign cystic disease (n = 3), a contralateral lesion diagnosed as IDC (n = 1), a segmentally distributed pattern diagnosed as atypical ductal hyperplasia (n = 1), and non-specific scattered calcifications (n = 1). Contrast enhancement was observed on CEM in all 4 microcalcification-associated ILC cases and the single IDC case. In contrast, benign-appearing calcifications showed no enhancement. Notably, although MRI confirmed the enhancement in malignant cases, it failed to visualize or verify the microcalcifications themselves in any of the 10 patients.

Architectural distortion was observed in 44 lesions (71%) on CESM and was absent in 18 lesions (29%). According to the CEM conspicuity classification, 13 lesions (21%) demonstrated low conspicuity, 17 lesions (27.4%) moderate conspicuity, and 32 lesions (51.6%) high conspicuity (Table 1).

Enhancement kinetics CEM revealed 19 lesions (30.6%) with type 1, 37 lesions (59.7%) with type 2, and 6 lesions (9.7%) with type 3 enhancement. On MRI, 17 lesions (27.4%) were type 1, 37 (59.7%) type 2, and 8 (12.9%) type 3. There was a statistically significant level of agreement between CEM and MRI kinetic curve patterns (Kappa: 0.764; $P < 0.001$). Compared with MRI, CEM showed sensitivity values of 94.1% for type 1, 89.2% for type 2, and 62.5% for type 3. Positive predictive values of CEM vs. MRI were 84.2% for type 1, 89.2% for type 2, and 83.3% for type 3 (Table 2).

When evaluating the relationship between architectural distortion and MRI enhancement kinetics, architectural distortion was seen in 41.2% of MRI type 1 lesions, 78.4% of type 2, and 100.0% of type 3. The proportion in type 1 was statistically lower than in types 2 and 3, although there was no significant difference between type 2 and type 3 (Table 3).

Similarly, when architectural distortion was evaluated in relation to CEM enhancement kinetics types, distortion was observed in 42.1% of type 1 lesions, 83.8% of type 2, and 83.3% of type 3. Again, distortion was statistically lower in type 1 compared with types 2 and 3, with no significant difference between types 2 and 3 (Table 4).

Regarding MRI conspicuity levels, low conspicuity was noted in 52.9% of type 1, 10.8% of type 2, and 0% of type 3 lesions. Low conspicuity was significantly higher in type 1 than in types 2 and 3. High conspicuity was present in 5.9% of type 1, 62.2% of type 2, and 100.0% of type 3 lesions, being significantly lower in type 1. There was no significant difference between types 2 and 3 in terms of low or high conspicuity. Moderate conspicuity showed no statistically significant differences among the three types (Table 3).

In CEM, low conspicuity was observed in 57.9% of type 1, 5.4% of type 2, and 0% of type 3 lesions. Low conspicuity in type 1 was significantly higher than in types 2 and 3, with no significant difference between types 2 and 3. High conspicuity was noted in 0% of type 1, 70.3% of type 2, and 100.0% of type 3 lesions. High conspicuity in type 1 was statistically lower than in types 2 and 3, with no significant difference between types 2 and 3. Moderate conspicuity did not differ significantly between CEM enhancement kinetics types (Table 4) (Figures 2 and 3).

Discussion

ILC frequently demonstrates multifocal, multicentric, or bilateral involvement compared with other breast cancer subtypes due to its unique growth pattern and lack of a significant stromal response. Because ILC often exhibits an infiltrative growth pattern without forming a discrete mass, its detection by conventional MG and ultrasonography can be particularly challenging, especially in patients with dense breast parenchyma.[1,3,7-9]

Breast MRI is widely used for preoperative staging of ILC owing to its high sensitivity in detecting additional ipsilateral and contralateral lesions.[7,10] However, MRI is limited by lower specificity, contraindications, longer acquisition times, and higher costs, restricting its use in some patients.[1,2,5] CEM, by comparison, offers the combined advantages of lower cost, shorter examination time, and the ability to provide both functional and morphological information, making it an attractive alternative imaging modality.[2,4,8]

In this retrospective study, we compared CEM and MRI findings in histopathologically confirmed ILC cases in terms of morphological patterns, lesion size, enhancement kinetics, architectural distortion, and lesion conspicuity.

Our study demonstrated that CEM and MRI have comparable performance in iden-

Table 1. Lesion-based statistics (n = 62)

Variables	Statistics, n (%)
Enhancement kinetics (CEM)	
Type 1	19 (30.6)
Type 2	37 (59.7)
Type 3	6 (9.7)
Enhancement kinetics (magnetic resonance imaging)	
Type 1	17 (27.4)
Type 2	37 (59.7)
Type 3	8 (12.9)
Architectural distortion	
Present	44 (71.0)
Absent	18 (29.0)
Conspicuity	
Low	13 (21.0)
Moderate	17 (27.4)
High	32 (51.6)
Mass	
Absent	18 (29.0)
Present	44 (71.0)
Non-mass enhancement	
Absent	31 (50.0)
Present	31 (50.0)
Small mass	
Absent	39 (62.9)
Present	23 (37.1)
Microcalcification*, (CEM)	
Absent	36 (78.3)
Present	10 (21.7)

*Microcalcification data are presented on a patient basis. n, number of lesions; %, percentage value; CEM, contrast-enhanced mammography.

Table 2. Inter-modality agreement between magnetic resonance imaging and contrast-enhanced mammography enhancement kinetics classification

	MRI type 1	MRI type 2	MRI type 3	Total	Kappa coefficient	*P* value
CEM type 1 (n)	16	3	0	19	**0.764**	**< 0.001**
% within CEM	84.2	15.8	0.0	100.0		
% within MRI	94.1	8.1	0.0	30.6		
CEM type 2 (n)	1	33	3	37		
% within CEM	2.7	89.2	8.1	100.0		
% within MRI	5.9	89.2	37.5	59.7		
CEM type 3 (n)	0	1	5	6		
% within CEM	0.0	16.7	83.3	100.0		
% within MRI	0.0	2.7	62.5	9.7		
Total (n)	17	37	8	62		
% within CEM	27.4	59.7	12.9	100.0		
% within MRI	100.0	100.0	100.0	100.0		

Kappa coefficient calculated using Cohen's kappa test. Kappa interpretation reference:[19]; n number of lesions; CEM, contrast-enhanced mammography; MRI, magnetic resonance imaging.

tifying index lesions and measuring lesion size, with no statistically significant differences between the two modalities. Similar findings in the literature indicate that both CEM and MRI show high accuracy in lesion size estimation, though both tend to slightly overestimate tumor size compared with pathology.[8] This mild overestimation, however, was not clinically significant and did not impact surgical planning.

Fallenberg et al.[11] reported that the accuracy of CEM in estimating tumor size compared with MRI can be explained by several factors, most notably the high BPE observed on MRI, which may artificially increase the measured tumor size. Similarly, Fakhry et al.[2] found that MRI tended to overestimate tumor extension compared with CEM when correlated with histopathology. In agreement with Patel et al.,[12] Amato et al.[4] also demonstrated that CEM provides reliable measurements of the maximum diameter of the index lesion, showing strong concordance with final histopathological sizes.

In our study, conspicuity patterns were closely associated with enhancement kinetics. Lesions demonstrating type 1 kinetics tended to exhibit lower conspicuity, whereas type 2 and type 3 patterns were generally associated with more prominent enhancement. This relationship likely reflects differences in tumor vascularity and stromal response among the kinetic subtypes.

Architectural distortion detected on low-energy CEM images may or may not be associated with enhancement. Previous studies have suggested that benign and malignant distortions could potentially be differentiated based on enhancement patterns; however, current evidence remains insufficient to make this distinction reliably.[12] Therefore, when architectural distortion persists on low-energy images as well as on conventional MG and tomosynthesis, percutaneous biopsy is recommended regardless of enhancement characteristics.[6]

In our study, architectural distortion was more frequently observed in lesions demonstrating type 2 and type 3 enhancement kinetics on both CEM and MRI. This finding may reflect increased stromal changes and higher vascularization in these lesions. Consistent with our results, Amato et al.[4] reported that CEM performed comparably with MRI in detecting multifocal or multicentric disease and architectural distortions.

ILC differs from IDC in its infiltrative and discohesive growth pattern and is less fre-

Table 3. Associations between breast magnetic resonance imaging enhancement kinetics and lesion morphologic features

	MRI type 1 n (%)	MRI type 2 n (%)	MRI type 3 n (%)	Test value	*P* value
Architectural distortion					
Present	7 (41.2)[a]	29 (78.4)[b]	8 (100.0)[b]	10.705	0.004¥
Absent	10 (58.8)[a]	8 (21.6)[b]	0 (0.0)[b]		
Conspicuity					
Low	9 (52.9)[a]	4 (10.8)[b]	0 (0.0)[b]		
Moderate	7 (41.2)[a]	10 (27.0)[a]	0 (0.0)[a]	26.153	< 0.001¥
High	1 (5.9)[a]	23 (62.2)[b]	8 (100.0)[b]		

Superscript letters a and b indicate statistically significant group differences within each row. Groups sharing the same superscript do not differ significantly. n, number of lesions; %, column percentage; ¥, Fisher–Freeman–Halton exact test; CEM, contrast-enhanced mammography.

Table 4. Associations between contrast-enhanced mammography enhancement kinetics and morphologic features

	CEM type 1 n (%)	CEM type 2 n (%)	CEM type 3 n (%)	Test value	*P* value
Architectural distortion					
Present	8 (42.1)[a]	31 (83.8)[b]	5 (83.3)[b]	10.203	0.005¥
Absent	11 (57.9)[a]	6 (16.2)[b]	1 (16.7)[b]		
Conspicuity					
Low	11 (57.9)[a]	2 (5.4)[b]	0 (0.0)[b]		
Moderate	8 (42.1)[a]	9 (24.3)[a]	0 (0.0)[a]	38.132	< 0.001¥
High	0 (0.0)[a]	26 (70.3)[b]	6 (100.0)[b]		

Superscript letters a and b indicate statistically significant differences within the same row. Groups sharing the same superscript do not differ significantly. n, number of lesions; %, column percentage; ¥, Fisher–Freeman–Halton exact test; CEM, contrast-enhanced mammography.

quently associated with microcalcifications. Accordingly, ILC may be mammographically occult or present only as a subtle architectural distortion, which can lead to an underestimation of disease extent when relying solely on conventional morphological features. Therefore, functional imaging modalities such as CEM and MRI, by highlighting tumor-associated vascularity, provide a more comprehensive assessment of lesion distribution and preoperative staging in ILC. This underlines the rationale for our study's focus on contrast enhancement patterns and kinetics, rather than relying solely on standard morphological features.[1,13,14]

Whereas CEM evaluation is limited to the breast tissue itself, MRI additionally enables assessment of the axilla, chest wall, and internal mammary lymph nodes.[8] Pereslucha et al.[1] demonstrated that CEM does not contribute to axillary staging and cannot visualize internal mammary lymph nodes. Similarly, in our study, the detection of extramammary lymph nodes was significantly higher on MRI (21.7%) than on CEM. However, detection rates of IDC or other associated breast pathologies were comparable between modalities.

Although microcalcifications are less characteristic of ILC compared with ductal subtypes, they were identified in 21.7% of our cohort (n = 10). Our findings highlight a key intrinsic advantage of CEM over MRI: the capability to evaluate simultaneously morphological calcifications on low-energy images and functional enhancement on recombined images. In our series, CEM demonstrated enhancement in all malignant lesions associated with microcalcifications (including ILC and contralateral IDC), whereas benign-appearing scattered calcifications remained non-enhancing. As expected, MRI failed to visualize or verify these microcalcifications directly in any case, providing only enhancement data. These observations suggest that CEM offers complementary diagnostic value by depicting subtle calcific features that remain occult on MRI, thereby contributing to a more comprehensive preoperative assessment of ILC and associated pathologies.

Among 17 patients (37%) with axillary lymph node involvement, nodes were similarly detected by both CEM and MRI, although MRI allowed clearer visualization owing to its superior soft-tissue contrast. Given that many ILC cases present without palpable masses, the integration of CEM into our routine screening protocol, particularly during synchronous MG and ultrasonography, has improved our detection of axillary lymph nodes in daily practice. Nevertheless, internal mammary lymph nodes and chest wall involvement remain better evaluated with MRI.

In our cohort, mass enhancement was the most common presentation on both CEM and MRI, followed by NME. This distribution is consistent with the known infiltrative growth pattern of ILC. Fakhry et al.[2] reported NME as the most frequently observed enhancement pattern on both modalities, followed by isolated masses on CEM and combined NME/mass patterns on MRI. In our study, CEM successfully detected even subtle low-level enhancements, and comparable lesion identification between CEM and MRI may be attributed to our extensive institutional experience with CEM in routine practice.

Amato et al.[4] demonstrated that the presence of NME reduced the sensitivity of CEM for detecting additional lesions to as low as 25%, whereas cases involving isolated masses or combined mass/NME patterns achieved 100% sensitivity. In our study, this limitation was not observed, likely due to our ability to categorize small satellite nodules and associated NME separately, improving CEM's diagnostic performance. Our decision to focus on the largest non-index lesion allowed for a more meaningful assessment of clinically significant additional disease. This approach reflects real-world surgical decision-making, where the largest additional focus typically dictates the transition from breast-conserving therapy to more extensive surgical interventions.

The assessment of enhancement kinetics on CEM remains inherently limited compared with dynamic contrast-enhanced MRI, as CEM does not provide continuous temporal acquisition. However, prior studies have demonstrated that phase-based evaluation of enhancement changes can provide a reasonable approximation of kinetic behavior. In particular, kinetic patterns derived from CEM have been shown to correlate with MRI kinetic curve types and can be classified using analogous categories, such as persistent, plateau, and washout. Therefore, in the present

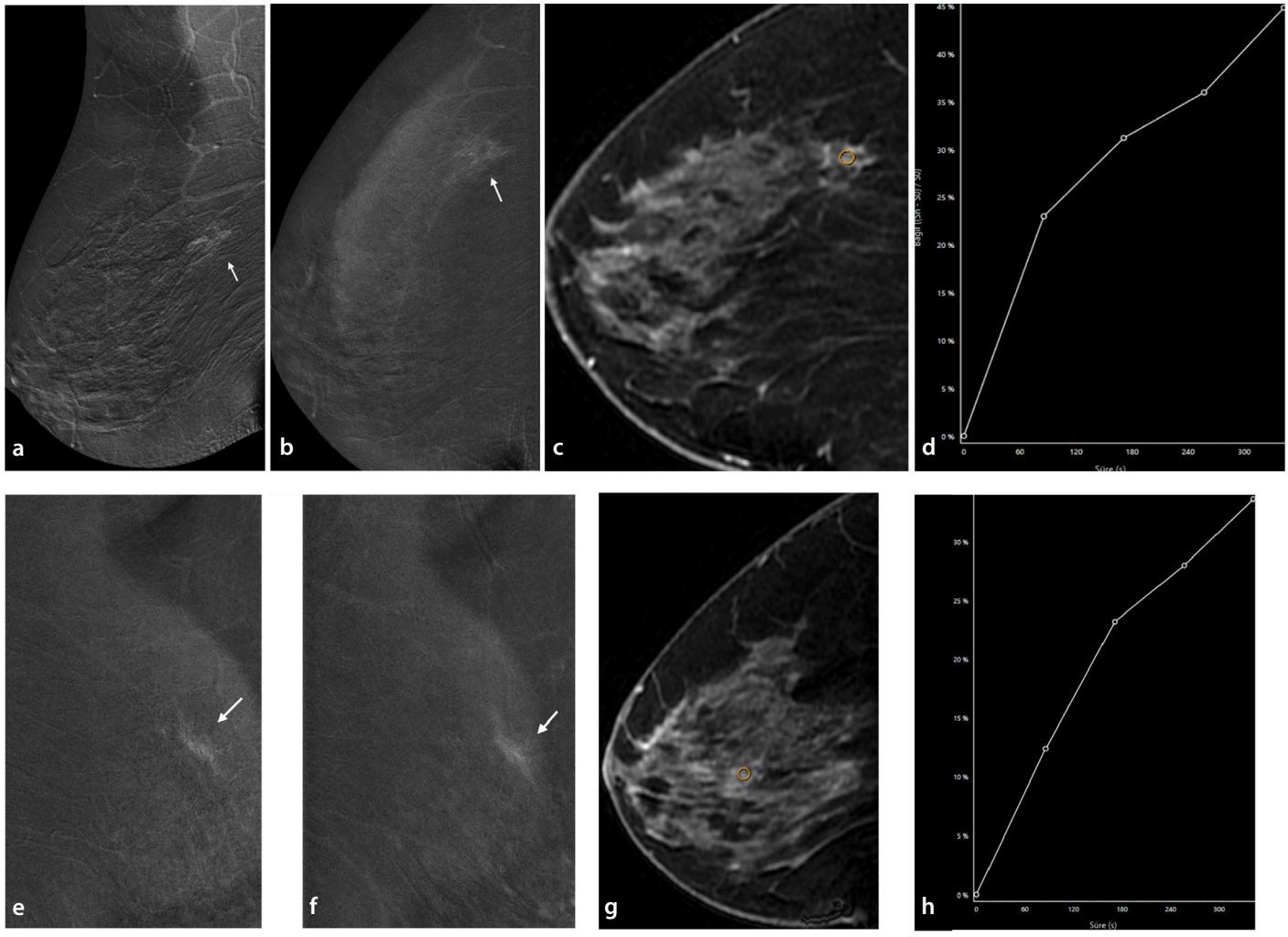

Figure 2. A 62-year-old female patient with non-mass enhancement (NME). On contrast-enhanced mammography (CEM), an ill-defined parenchymal distortion is seen in the right breast at the 2 o'clock position, measuring 2 × 1.5 cm **(a)**, demonstrating subtle delayed-phase (5th minute) enhancement **(b)**. Corresponding breast magnetic resonance imaging (MRI) shows NME with a type 1 kinetic curve in the same location **(c, d)**. Left breast, CEM reveals additional NME in the retroareolar region and at the 1 o'clock position, approximately 5 cm from the areola **(e, f)**, which are confirmed on MRI with type 1 enhancement kinetics **(g, h)**.

study, we adopted a phase-based approach using early and delayed images to characterize enhancement kinetics. Although this method does not fully replicate MRI dynamic analysis, it allows a practical and clinically applicable assessment of lesion behavior on CEM. Furthermore, this phase-based kinetic assessment, when considered together with CEM's intrinsic ability to detect associated microcalcifications, may provide complementary diagnostic information despite the lack of continuous temporal data.[15,16] Our study found a high level of agreement between CEM and MRI in classifying enhancement kinetics (Kappa: 0.764; $P < 0.001$). These findings are consistent with Fakhry et al.,[2] who also reported strong concordance between the two modalities in ILC assessment. Moreover, CEM demonstrated high sensitivity for distinguishing enhancement kinetics curve types—94.1% for type 1, 89.2% for type 2, and 62.5% for type 3—which aligns with previous reports indicating that CEM provides diagnostic accuracy comparable with MRI.[7]

Because radiation exposure is always a concern, it is important to assess whether CEM alone offers diagnostic efficacy comparable with combined CEM and digital MG. In CEM, the total X-ray dose delivered for dual-energy imaging varies according to breast thickness and tissue composition. The average glandular dose for low-energy CEM images is equivalent to that of conventional MG, whereas high-energy images correspond to approximately 20% of the conventional MG dose in contrast-optimized modes. In line with recent studies, our findings indicate that the diagnostic performance of CEM alone is not inferior to CEM combined with MG.[17,18] Therefore, the additional radiation exposure associated with CEM can be considered clinically acceptable in appropriately selected patients, particularly when balanced against its diagnostic benefits.

Our study has several limitations. First, its retrospective, single-center design may limit the generalizability of the findings. Second, definitive lesion size verification using surgical pathology was not possible in patients receiving neoadjuvant chemotherapy due to treatment-induced tumor regression. In these cases, size comparisons relied on radiological findings. Third, microcalcifications were not analyzed as a primary study endpoint; although detected and correlated, their diagnostic impact requires further validation in larger cohorts. Fourth, breast MRI was performed regardless of the menstrual cycle phase, which may have influenced BPE and lesion conspicuity in premenopausal patients. Finally, clinical outcome parameters, such as long-term re-excision rates and changes in surgical planning, were not systematically evaluated. Future prospective, multicenter studies are warranted to refine the diagnostic role of CEM in ILC further.

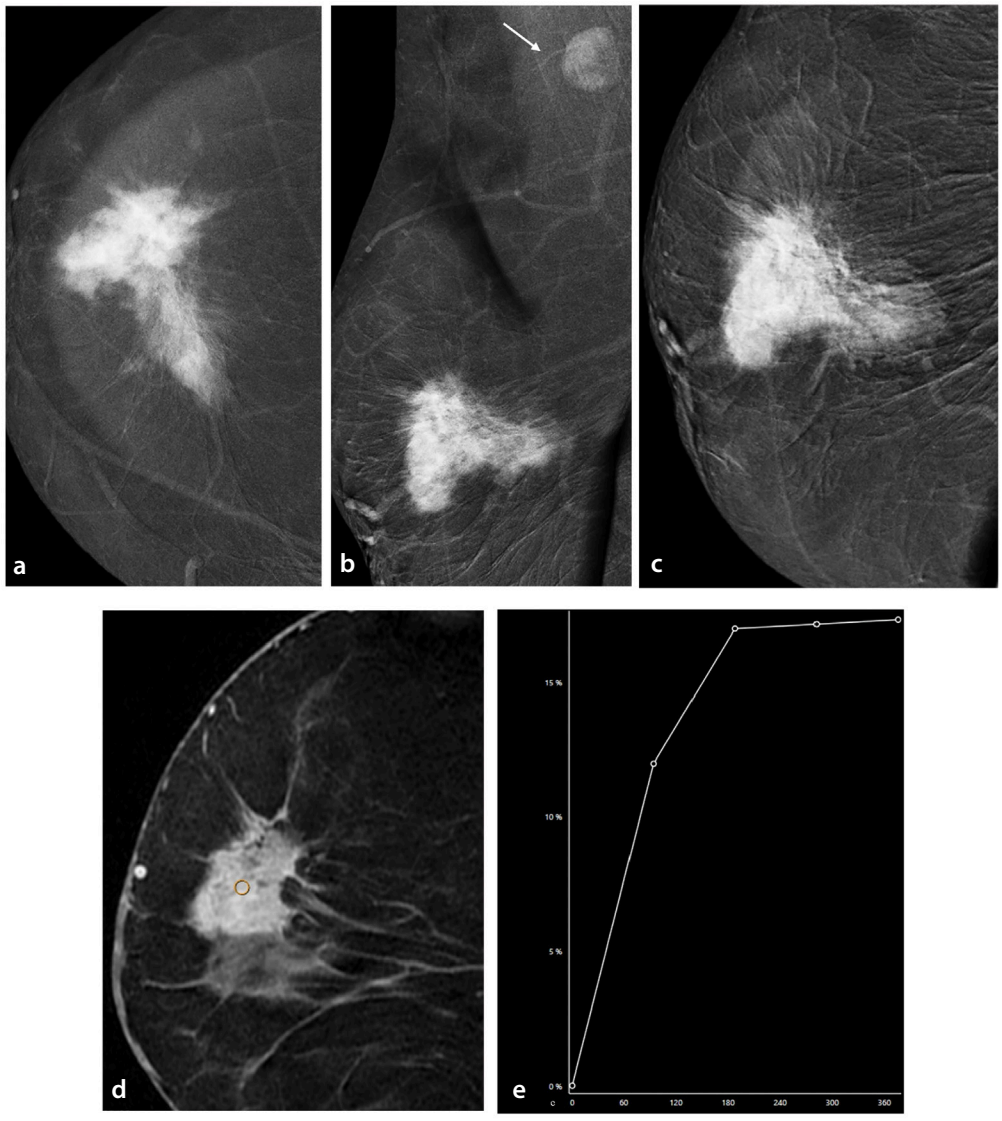

Figure 3. An American College of Radiology Breast Imaging Reporting and Data System 5 mass in the right breast at the 12 o'clock periareolar region demonstrates spiculated margins, high conspicuity, parenchymal distortion, nipple retraction, and tethering of the Cooper ligaments on contrast-enhanced mammography (CEM). The lesion exhibits intense enhancement without definite washout on the 4-minute delayed phase image **(a–c)**. Correspondingly, breast magnetic resonance imaging reveals an irregular mass with a type 2 kinetic curve in the same location **(d, e)**. A right axillary lymph node with cortical thickening is visualized on CEM **(b)**.

CEM represents a valuable alternative imaging modality in ILC, especially in patients where MRI is contraindicated or inaccessible. However, MRI remains the gold standard for characterizing certain enhancement patterns, particularly NME. Future studies with larger patient cohorts and comprehensive histopathological correlation are warranted to further refine the diagnostic role of CEM in ILC and its impact on surgical planning and patient outcomes.

Footnotes

Conflict of interest disclosure

The authors declared no conflicts of interest.

References

1. Pereslucha AM, Wenger DM, Morris MF, Aydi ZB. Invasive lobular carcinoma: a review of imaging modalities with special focus on pathology concordance. *Healthcare (Basel)*. 2023;11(5):746. [Crossref]
2. Fakhry S, Kamal RM, Nada OM, Mohamed AEAE, Hanafy MM. A comparative study between the diagnostic performance of contrast-enhanced digital mammography and dynamic contrast-enhanced MRI in invasive lobular carcinoma of the breast. *Egypt J Radiol Nucl Med*. 2024;55:31. [Crossref]
3. Arpino G, Bardou VJ, Clark GM, Elledge RM. Infiltrating lobular carcinoma of the breast: tumor characteristics and clinical outcome. *Breast Cancer Res*. 2004;6(3):R149-R156. [Crossref]
4. Amato F, Bicchierai G, Cirone D, et al. Preoperative loco-regional staging of invasive lobular carcinoma with contrast-enhanced digital mammography (CEDM). *Radiol Med*. 2019;124(12):1229-1237. [Crossref]
5. Mann RM. The effectiveness of MR imaging in the assessment of invasive lobular carcinoma of the breast. *Magn Reson Imaging Clin N Am*. 2010;18(2):259-276, ix. [Crossref]
6. American College of Radiology. ACR BI-RADS® v2025 manual: *Breast imaging reporting and data system*. Reston (VA): American College of Radiology; 2025. [Crossref]
7. Xing D, Lv Y, Sun B, et al. Diagnostic value of contrast-enhanced spectral mammography in comparison to magnetic resonance imaging in breast lesions. *J Comput Assist Tomogr*. 2019;43(2):245-251. [Crossref]

8. Costantini M, Montella RA, Fadda MP, et al. Diagnostic challenge of invasive lobular carcinoma of the breast: what is the news? Breast magnetic resonance imaging and emerging role of contrast-enhanced spectral mammography. *J Pers Med*. 2022;12(6):867. [Crossref]
9. Chen Z, Yang J, Li S, et al. Invasive lobular carcinoma of the breast: a special histological type compared with invasive ductal carcinoma. *PLoS One*. 2017;12(9):e0182397. [Crossref]
10. Mann RM, Cho N, Moy L. Breast MRI: state of the art. *Radiology*. 2019;292(3):520-536. [Crossref]
11. Fallenberg EM, Dromain C, Diekmann F, et al. Contrast-enhanced spectral mammography versus MRI: initial results in the detection of breast cancer and assessment of tumour size. *Eur Radiol*. 2014;24(1):256-264. [Crossref]
12. Patel BK, Naylor ME, Kosiorek HE, et al. Clinical utility of contrast-enhanced spectral mammography as an adjunct for tomosynthesis-detected architectural distortion. Clin Imaging. 2017;46:44-52. [Crossref]
13. Lobbes MBI, Neeter LMFH, Raat F, et al. The performance of contrast-enhanced mammography and breast MRI in local preoperative staging of invasive lobular breast cancer. *Eur J Radiol*. 2023;164:110881. [Crossref]
14. Giannotti E, Van Nijnatten TJA, Chen Y, et al. The role of contrast-enhanced mammography in the preoperative evaluation of invasive lobular carcinoma of the breast. *Clin Radiol*. 2024;79(6):e799-e806. [Crossref]
15. Rong X, Kang Y, Xue J, Han P, Guang Y, Li Z. Contrast-enhanced spectral mammography: are kinetic patterns useful for differential diagnoses of enhanced lesions? *Diagn Interv Radiol*. 2023;29(2):244-250. [Crossref]
16. Xu W, Zheng B, Chen W, et al. Can the delayed phase of quantitative contrast-enhanced mammography improve the diagnostic performance on breast masses? *Quant Imaging Med Surg*. 2021;11(8):3684-3697. [Crossref]
17. Łuczyńska E, Heinze-Paluchowska S, Hendrick E, et al. Comparison between breast MRI and contrast-enhanced spectral mammography. *Med Sci Monit*. 2015;21:1358-1367. [Crossref]
18. Fallenberg EM, Schmitzberger FF, Amer H, et al. Contrast-enhanced spectral mammography vs. mammography and MRI - clinical performance in a multi-reader evaluation. *Eur Radiol*. 2017;27(7):2752-2764. [Crossref]
19. McHugh ML. Interrater reliability: the kappa statistic. *Biochem Med (Zagreb)*. 2012;22(3):276-282. [Crossref]